



TerraGreen 13 International Conference 2013 - Advancements in Renewable Energy and Clean Environment

Electric Automobile Ni-MH Battery Investigation in diverse situations

Brahim Mebarki^{a,*}, Belkacem Draoui^b, Lakhdar Rahmani^c, Boumediène Allaoua^d

^aDepartment of Technology, Faculty of the Sciences and Technology, BECHAR University, B.P 417 BECHAR (08000), ALGERIA.

^bLaboratory of Energy in Arid Region (ENERGARID), BECHAR University, B.P 417 BECHAR (08000), ALGERIA.

^cDepartment of Technology, Faculty of the Sciences and Technology, BECHAR University, B.P 417 BECHAR (08000), ALGERIA.

^dDepartment of Technology, Faculty of the Sciences and Technology, BECHAR University, B.P 417 BECHAR (08000), ALGERIA.

Abstract

The electronic differential system ensures the robust control of the vehicle compartment on the road. This paper focuses Ni-MH Battery controlled by Buck Boost DC-DC converter power supply for EV. Sliding mode control based on space vector modulation (SVM-SMC) is proposed to achieve the tow rear driving wheel control. The performances of the proposed strategy controller give a satisfactory simulation results. The proposed control law increases the utility EV autonomous under several speed variations. Moreover, the future industrial's vehicle must take into considerations the battery material choice into design steps. The battery material model choice is a crucial item, and thanks to an increasing emphasis on vehicle range and performance, the Ni-MH battery could become a viable candidate that's our proposal battery model in the present work, in this way the present paper show a novel strategy of electric automobile (EA) power electronics studies when the current battery take into account the impact of the sliding mode control based onspace vector machine technique in the several speed variations using the primitive battery SOC of 60% state.

© 2013 The Authors. Published by Elsevier Ltd. Open access under [CC BY-NC-ND license](http://creativecommons.org/licenses/by-nc-nd/3.0/).

Selection and/or peer-review under responsibility of the TerraGreen Academy

Keywords: State of Charge, Ni-MH battery, power, DC-DC Buck-Boost converter, SVM-SMC, electric automobile.

1. Introduction

Nickel metal hydride (Ni-MH) batteries have dominated the automotive application since 1990's due to their overall performance and best available combination of energy and power densities, thermal performance and cycle life. They do not need maintenance, require simple and inexpensive charging and

* Corresponding author. Tel.: +213.661.963.537 ;Fax: 00 213 49 81 52 44

E-mail address: brahimo12002@yahoo.fr.

electronic control and are made of environmentally acceptable recyclable materials. The capacity of NiMH cell is relatively high but its cell potential is 1.35 V. The gravimetric energy density is about 95 Wh/kg and volumetric energy is about 350 Wh/L [1-3].

Battery technology is one of most important areas of research pertaining to the reliability and commercial popularity of this alternative form of transportation. The battery forms a very crucial component of the drive train [3]. It provides the desired electric power to the traction motor in accordance with the driver's requirement. The battery properties widely vary with the chemistry. The battery should be capable of storing sufficient energy, offer high energy efficiency, high current discharge, and good charge acceptance from regenerative braking, high cycle time and calendar life and abuse tolerant capability. It should also meet the necessary temperature and safety requisites.

Electric vehicle, which address the “drive performance” issue, may provide a more feasible opportunity for nickel metal hydride battery technology. Thanks to an increasing emphasis on vehicle range and battery energy density, Nickel metal hydride could become a viable candidate. The greatest advantages are the high cell voltage compared with nickel technology) and superior energy density. Other attractive features are a very low self-discharge rate and no memory effect.

The sliding mode control strategy (SMC) is one kind of high performance driving technologies for AC motors, due to its simple structure and ability to achieve fast response of flux and torque has attracted growing interest in the recent years. SMC-SVM with PI controller sliding mode control without hysteresis band can effectively reduce the torque ripple, but its system's robustness will be further enhanced. SMC-SVM method can improve the system robustness, evidently reduce the torque and flux ripple, and effectively improve the dynamical performance. The DC-DC converter is used with a control strategy to assure the energy required for the EV and the propulsion system.

State of charge (SOC) symbolizes the residual capacity of battery and is written as the residual capacity percent by nominal capacity. The estimation of SOC of any battery is a key point of energy in EV management system, in this paper we study the NiMH ability to become an energy source candidate for the next future electric vehicle by testing its power state changes performances under several speed driver conditions [2,3].

2. Electric Vehicle description

According to Fig. 1 the opposition forces acting to the vehicle motion are: the rolling resistance force F_{tire} due to the friction of the vehicle tires on the road; the aerodynamic drag force F_{aero} caused by the friction on the body moving through the air; and the climbing force F_{slope} that depends on the road slope [1,2,3]. The total resistive force is equal to F_r and is the sum of the resistance forces, as in (1).

$$F_r = F_{\text{tire}} + F_{\text{aero}} + F_{\text{slope}} \quad (1)$$

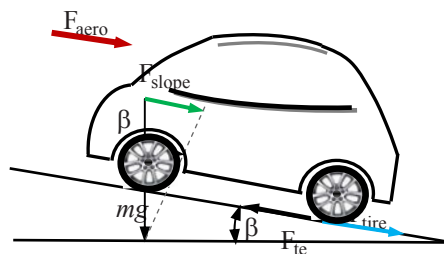


Fig. 1. The forces acting on a vehicle moving along a slope.

The vehicle considered in this work is two-rear-wheels drive EV destined to urban transportation. Two induction motors are coupled in each of the rear wheels. The energy source of the electric motors comes from the NI-MH battery controller by Buck boost DC-DC converter [2,9].

3. Ni-MH description

The following equations (2) provide basic cell reactions of a NiMH battery. In a fully charged state, the active material on the positive electrode is Nickel oxy-hydroxide and that on the negative electrode is metal hydride. During the charge reaction, hydroxide from the electrolyte reacts with the nickel oxy-hydroxide Ni(OH)₂ found on the positive electrode to form NiOOH and water, while, on the negative electrode, water reacts with the metal alloys to form metal hydride. The charge reaction is exothermic. The heat produced during the charge process must be released to avoid continuous temperature rise of the cells [5-2-1].

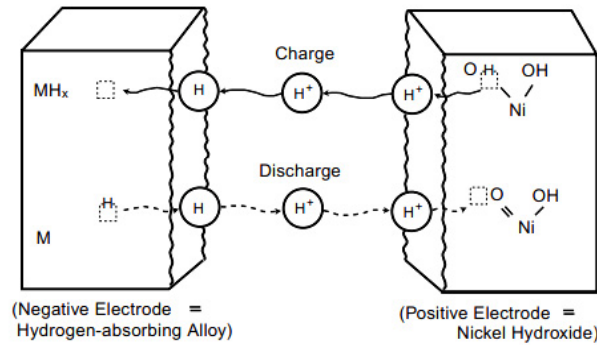


Fig.2 .Basic chemistry reaction for of nickel-metal hydride battery



Fig 3. describe the equivalent circuit of Nickel metal hydride battery where, E is the no load voltage ; E₀ is the constant voltage; K is the polarization constant or polarization resistance; Q is maximum battery capacity; Q is exponential voltage ; B is exponential capacity .All the parameter of the equivalent circuit type ,based on its discharge characteristics.

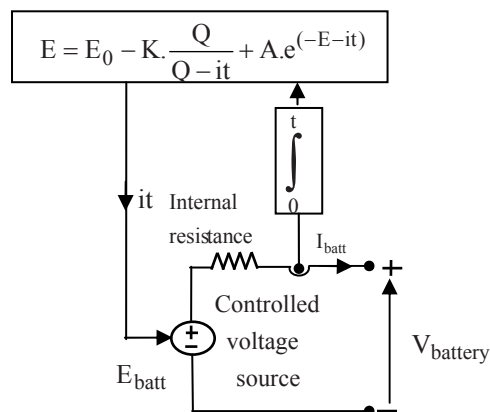


Fig. 3. The equivalent circuit of Nickel metal hydride battery

The State-Of-Charge (SOC) of the battery (between 0 and 100%). The SOC for a fully charged battery is 100% and for an empty battery is 0%. The SOC can be defined by equation (2):

$$SOC = 100 \left(1 - \frac{Q \cdot 1.05}{\int i \cdot dt} \right) \quad (3)$$

Fig.4 explain the different state of discharge curve, the first section represents the exponential voltage drop when the battery is charged. Depending on the battery type, this area is more or less wide. The second section represents the charge that can be extracted from the battery until the voltage drops below the battery nominal voltage. Finally, the third section represents the total discharge of the battery, when the voltage drops rapidly.

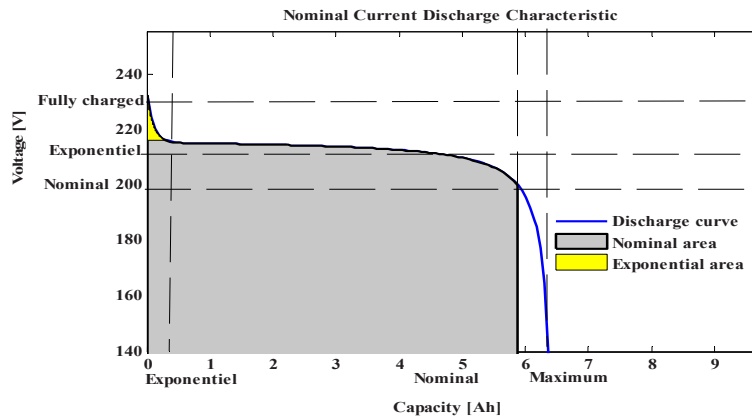


Fig. 4. Nickel metal hydride battery typical discharge curve.

The NiMH battery parameters using in the propulsion system proposed are illustrate in table blow.

Table 1. Nickel metal hydride parameter

Rated capacity	6.5 Ah
Nominal Voltage	1.18 V
Maximum Capacity	7 Ah
Nominal Discharge Current	1.3 A
Exponential Voltage	1.28 V
Internal Resistance	2 mΩ
Rated Capacity	6.5 Ah
Fully Charged voltage	1.39 V
Capacity Nominal Voltage	6.25 Ah
Exponential Capacity	1.3 Ah
Exponential Voltage	1.28 V

4. Sliding mode control strategy based space vector modulation (SVM-SMC)

The SVM technique has become one of the most important PWM methods for Voltage Source Inverter (VSI) since it gives a large linear control range, less harmonic distortion, fast transient response, and simple digital implementation [7].

The induction motor stator flux can be estimated by

$$S_1 = T^* - \hat{T} \quad (4) \quad \text{and} \quad S_2 = C(\hat{\psi}_r^* - \hat{\psi}_r) + (\hat{\psi}_r^* - \hat{\psi}_r) \quad (5)$$

$$u_\alpha = -k_1 \text{sign}(q_1) - k_2 q_1 \quad (6) \quad \text{and} \quad u_\beta = -k_1 \text{sign}(q_2) - k_2 q_2 \quad (7)$$

where $\text{sign}(q) = \begin{cases} +1, & q > 0 \\ -1, & q < 0 \end{cases}$; and k_1, k_2 are positive constants.

The SVM principle is based on the switching between two adjacent active vectors and two zero vectors during one switching period. It uses the space vector concept to compute the duty cycle of the switches. Fig. 5 shows a scheme of a three-phase two-level inverter with a star-connection load.

From Fig.6, the output voltages of the inverter can be composed by eight states $u_0, u_1 \dots u_7$, corresponding to the switch states $S_0(000), S_1(100), S_7(111)$, respectively. These vectors can be plotted on the complex plane ($\alpha\beta$) as shown in Fig.4, and are given by [3].

$$u_k = \begin{cases} \frac{2}{3} V_{dc} e^{j(k-1)(\pi/3)} & \text{for } k = 1, 2, \dots, 6 \\ 0 & \text{for } k = 0, 7 \end{cases} \quad (8)$$

The rotating voltage vector within the six sectors can be approximated by sampling the vector and switching between different inverter states during the sampling period. The vector u_s is commonly split into two nearest adjacent voltage vectors and zero u_0 and u_7 in an arbitrary sector. For example, during one sampling interval, vector u_s in sector I can be expressed as

$$u_s(t) = \frac{T_0}{T_s} u_0 + \frac{T_1}{T_s} u_1 + \frac{T_2}{T_s} u_2 + \frac{T_7}{T_s} u_7 \quad (9)$$

Where T_0, T_1, T_2, T_7 are the turn-on time of the vectors u_0, u_1, u_2, u_7 and T_s is the sampling time. $T_s - T_1 - T_2 = T_0 + T_7 \geq 0, T_0 \geq 0, T_7 \geq 0$.

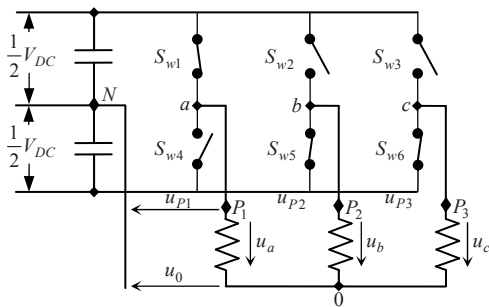


Fig. 5. Three phase two levels PWM inverter.

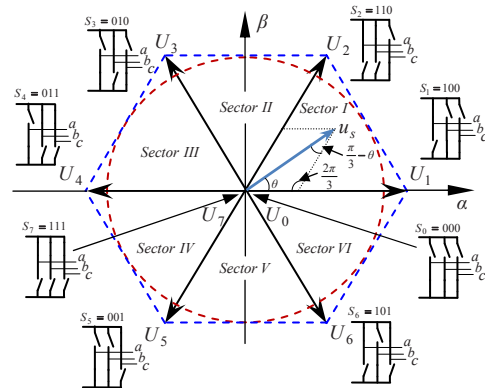


Fig. 6. Space vectors.

The block diagram of the SVM-SVM control scheme for voltage source inverter-fed IM is shown in Fig. 7. In this method two PI controllers are used for torque and flux regulation. The outputs of the PI flux and torque controllers generate the reference stator voltage components u_{qs}, u_{ds} , expressed in the stator flux

oriented coordinates (d–q). these components are dc voltage commands and then transformed into stationary coordinates (α–β). the commanded values $u_{s\alpha}, u_{s\beta}$ are delivered to space vector modulator (SVM), which generates switching signals S_a, S_b, S_c . for power transistors.

we can calculate u_{ds}^* and u_{qs}^* . by the flowing equation respectively:

$$u_{ds}^* = (K_{p\varphi} + \frac{K_{i\varphi}}{s})(\varphi - \varphi^*) \tag{10}$$

$$u_{qs}^* = (K_{pT_{em}} + \frac{K_{iT_{em}}}{s})(T_{em}^* - T_{em}^*) \tag{11}$$

5. Buck Boost DC-DC Converter for Electric Vehicle

DC-DC Buck boosts converters find applications in places where battery charging, regenerative braking, and backup power are required. The power flow in a bidirectional converter is usually from a low voltage end such as battery or a super capacitor to a high voltage side and is referred to as boost operation [6, 5]. Figure 7 show the electric vehicle propulsion chain using a DC-DC Buck boosts converters.

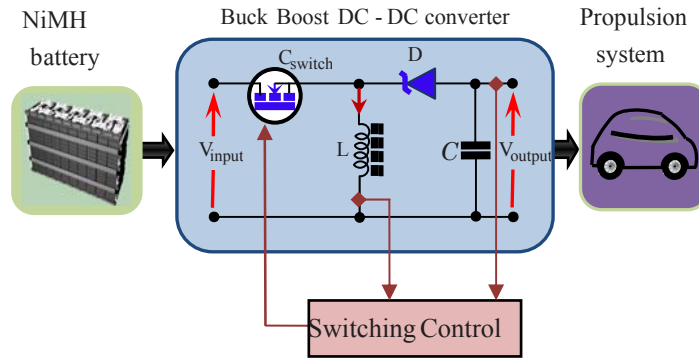


Fig. 7. The buck boost DC-DC converter control strategy scheme.

6. Simulation Results

In order to characterize the driving wheel system behaviour. The following results were simulated in MATLAB and its divided in two phases .the first one deal with the test of the EV performances controlled with SMC-SVM strategy under several speed variation in the other hand we show the impact of this controller on vehicle performance power electronics. Only the right motor simulations are shown. The assumption that the initialized Nickel metal hydride battery SOC is equal to 60%.

6.1. Sliding mode control scheme with space vector modulation.

The topology studied in this present work consists of three phases: the first one represent the acceleration phase’s beginning with 60 Km/h in straight road, the second phase represent the deceleration one when the speed became 30 Km/h, and finally the EV is moving up the sloped road of 10% under 80 Km/h, the specified road topology is shown in Fig. 8, when the speed road constraints are described in the Table 2.

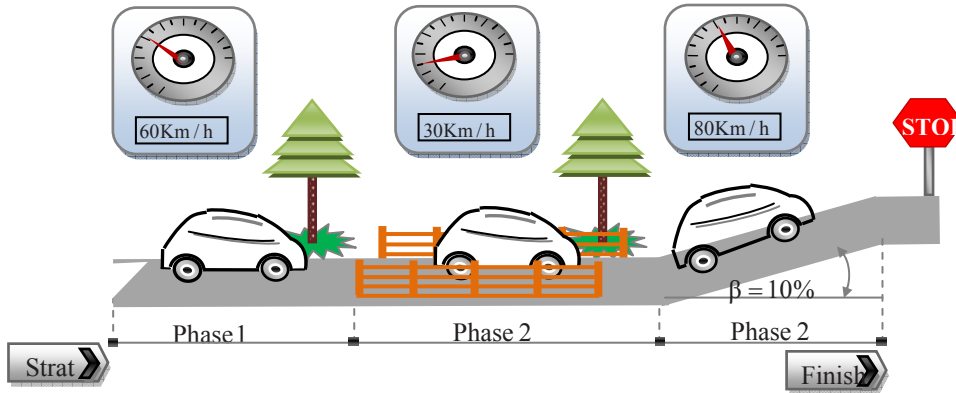


Fig. 8. Specified driving route topology.

Table 2. Specified driving route topology

Phases	Event information	Vehicle Speed[km/h]
Phase 1	Acceleration	60
Phase 2	Bridge, Break	30
Phase 3	Acceleration and climbing a slope 10%	80

Referred to Figure 9 at time of 2 s the vehicle driver move on straight road with linear speed of 60 km/h, the assumption's that the two motors are not disturbed and the Initial state of charge of 70 % is respected:

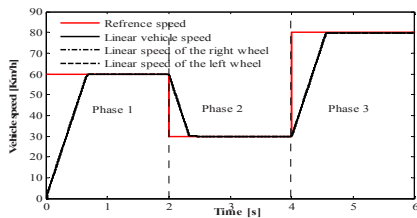


Fig.9. Variation of vehicle speeds. in different scenarios

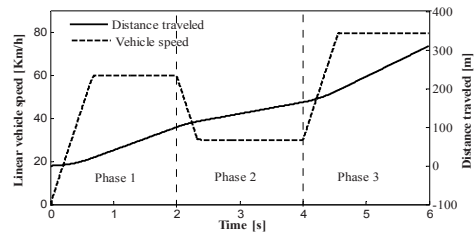


Fig.10. Variation of phase current of the right motor in different phases

Fig. 11, reflect the relationship between vehicle speed's variation and distance traveled in different phases. The distance travelled of 310 m in three electronic differential references acts 60 then break of 30 and acceleration until 80 km/h.

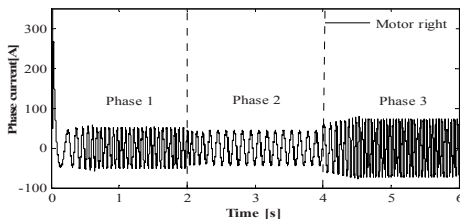


Fig.11. Variation of phase current of the right motor in different phases.

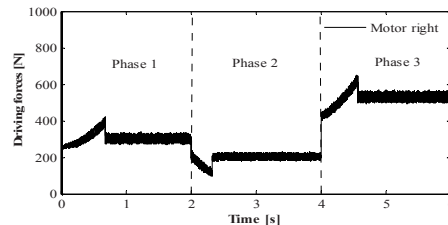


Fig.12. Variation of driving force of the right motor in different phases.

Figs 11 and 12 explains the variation of phase current and driving force respectively. In the first step and to reach 60 km/h The EV demand a current of 50.70 A for each motor which explained with driving force of 329.30N. In second phase the current and driving forces demand decreases by means that the vehicle is in recharging phase's which explained with the decreasing of current demand and developed driving forces shown in Figs 11 and 12 respectively . The last phases explain the effect of acceleration under the slope on the straight road EV moving. The driving wheels forces increase and the current demand undergo double of the current braking phases the battery use 80 % of his power to satisfy the motorization demand under the stopped road condition which can interpreted physically the augmentation of the globally vehicle resistive torque illustrate in Table 4. In the other hand the linear speeds of the two induction motors stay the same and the road drop does not influence the torque control of each wheels. The results are listed in Table 3.

Table 3. Values of phase current driving force of the right motor in different phases.

Phases	Phase 1	Phase 2	Phase 3
Current of the right motor [A]	50.71	44.21	70.78
Driving force of the right motor [N]	329.30	228.50	563.00

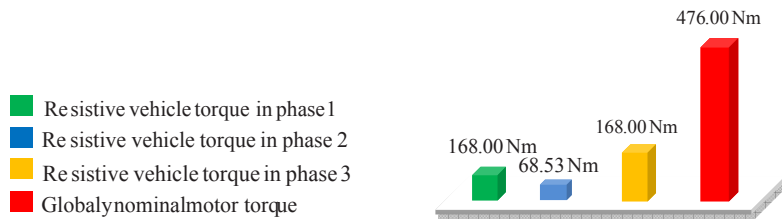


Fig.13. Evaluation of the globally vehicle torque compared to nominal motor torque in different phases.

According to the formulas (1), and Table. 4, the variation of resistive vehicle torques in different cases as depicted in Table 4. , the vehicle resistive torque was 95.31 N.m in the first case (acceleration phase) when the power propulsion system resistive one is only 68.53 Nm in the braking phases (phases 2) , the back driving wheels develop more and more efforts to satisfy the traction chain demand which impose an resistive torque equal to 168.00 N.m .The result prove that the traction chain under acceleration demand develop the double effort comparing with the breaking phase case's by means that the vehicle needs the half of its energy in the deceleration phase's compared with the acceleration one as it specified in table 4.

Table 4. Variation of vehicle torque in different Phases.

Phases	1	2	3
the Vehicle resistive torque [N.m]	95.31	68.53	168.00
the globally vehicle resistive torque Percent compared with nominal motor torque of 476 Nm	20.02 %	14.39 %	35.29 %

6.2. Power electronics.

The Nickel metal hydride battery must be able to supply sufficient power to the EV in accelerating and decelerating phase , which means that the peak power of the batteries supply must be greater than or at least equal to the peak power of the both electric motors. The battery must store sufficient energy to maintain their SOC at a reasonable level during driving, the Fig. 16 (a) and Fig. 16 (c) describes the changes in the battery storage power and current, voltage respectively in different speed references.

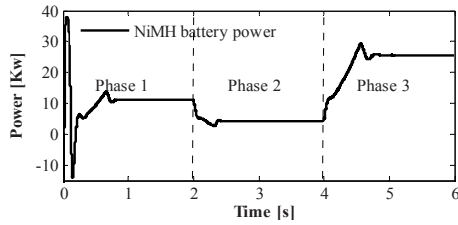


Fig.14. Variation of NiMH battery power in different phases

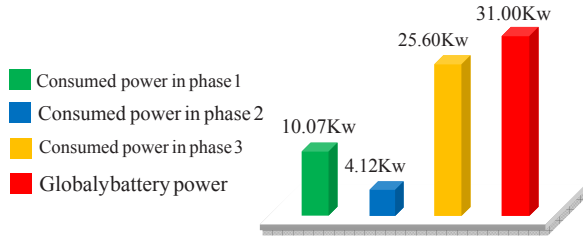


Fig.15. Variation of the maximum power battery power in different phases

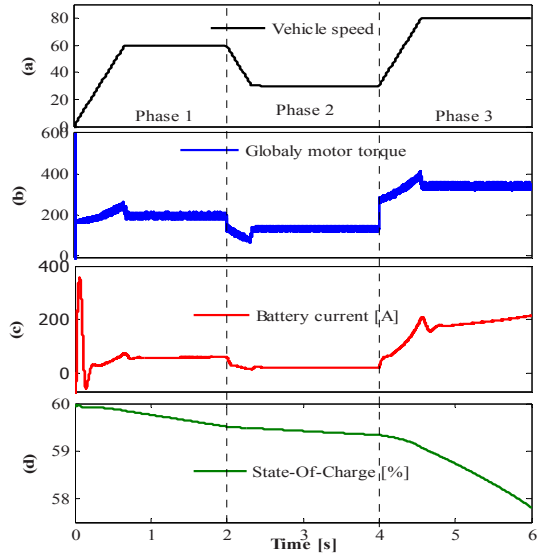


Fig.16. Variation of parameters during consideration scenario (a) vehicle speed, (b) globally motor power (c) battery current, and (c) SOC.

Table 5. Values of NiMH battery power in different phases.

Phase	Phase 1	Phase 2	Phase 3
Battery power [Kw]	10.07	4.12	25.60
Percentage of the battery power compared with globally motor power [%]	32.48	13.29	82.58

It is interesting to describe the power distribution in the electrical traction under several speed references. The battery provides about 11.07 Kw in the first phase in order to reach the electronic differential reference speed of 60 Km/h. In the second phase (phase 2: deceleration phase's) the demanded power battery decreased about 6.95 Kw that present 71.91% of the globally nominal power battery (31 Kw). In third phase the battery produced power is equal to 25.60 Kw under sloped road state. The used battery produced power depend only on the electronic differential consign by means the acceleration/deceleration driver state which can be explained by the battery SOC of Fig. 17.

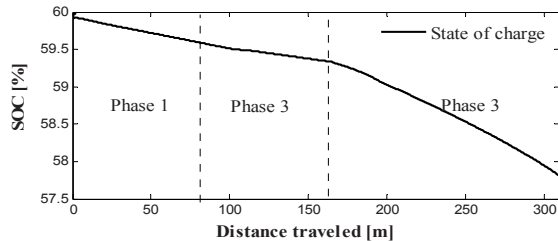


Fig.17. Battery efficiency versus state-of-charge.

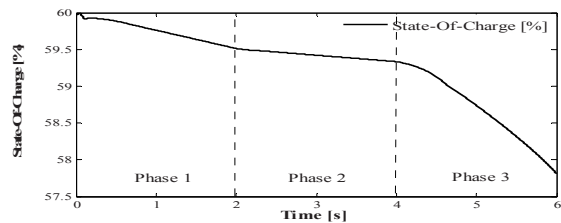


Fig.18. Variations of the SOC during traveled distance in versus vehicle speed.

Table 6. Evaluation of SOC [%] in the different phases.

Phase	Speed [Km/h]	Begin Phase [s]	End Phase[s]	SOC begin	SOC end	SOC diff
1	60	0	2	60.00	59.51	0.49
2	30	2	4	59.51	59.34	0.17
3	80	4	6	59.34	57.81	1.53

Fig. 18 explains how SOC (SOC) in the Nickel metal hydride battery changes during the driving cycle; it seems that the SOC decreases rapidly at acceleration, by means that the SOC range's between 57.81% to 60% during all cycle's phases from beginning at the end cycles. At $t = 6$ s, the battery SOC becomes lower than 57.82 % (it was initialized to 60 % at the beginning of the simulation). Table. 6 reflect the variation of SOC in different simulations phases. Figure 17 and 18 investigate the variation of sate of charge en function of vehicle speed and the traveled distance respectively. The relationship between SOC and left time in three phases are defined by the flowing linear fitting formula:

$$SOC[\%] = 0.0010147 t^6 - 0.014954 t^5 + 0.072173 t^4 - 0.12693 t^3 + 0.058746 t^2 + -0.1674 t + 59.978 \quad (10)$$

Moreover the simulation results specified by Figure 17, we can define the relationship between the sate of charge and the traveled distance in each cases, the first one (acceleration) is defined by the linear fitting formula:

$$SOC[\%] = -0.006 d_{traveled} + 60 \quad (11)$$

The second (deceleration) is obtained and represented by:

$$SOC[\%] = -0.0020 d_{traveled} + 59.67 \quad (12)$$




Finally the third phase's formula (acceleration under slope) is given by:

$$SOC[\%] = -0.01 d_{traveled} + 60.98 \quad (13)$$

Table 7. Evaluation of distance traveled and SOC

Phases	Phase 1	Phase 2	Phase 3
Distance traveled [m]	81.57	82.63	145.80
SOC Difference [%]	0.49	0.17	1.53
Total distance traveled	310.00 m		
Initial SOC [%]	60		
Final SOC [%]	57.81		

Table 8. The relationship between the traction chain power electronics characteristics and the distance traveled in different phases

	60Km/h 	30Km/h 	80Km/h 
	Phase 1	Phase 2	Phase 3
$D_{traveled}$ [m]	81.57	82.63	145.80
SOC_{diff} [%]	0.49	0.17	1.53
$P_{consumed}$ [Kw]	10.07	4.12	25.60

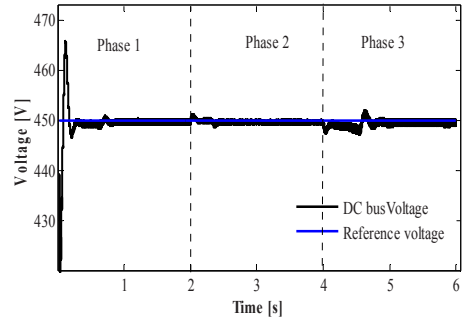


Fig.19. Robustness test of Buck Boost DC-DC converter under several speed.

This power is controlled by the Buck Boost DC-DC converter current and distribute accurately for three phases. From Fig. 19 we test the buck boost DC-DC converter robustness under several speed cycles. When the speed pass from 30 Km/h to 80 Km/h, the demanded voltage is 450 V. the buck boost converter is not only a robust converter which ensure the power voltage transmission but also a good battery recharger in deceleration state that help to perfect the vehicle autonomous with no voltage ripple ,the Table. 10 give voltage ripple in different cases in electrical traction system when the ripple rate changes are affected with the phase’s states.

Table 9. Evaluation of voltage ripple

Phases	1	2	3
The voltage ripple [V]	0.93 %	0.55%	1.03%

7. Conclusion

The power propulsion system studied in this paper has demonstrated that the Nickel metal hydride battery behavior controlled by buck boost DC-DC converter for utility EV which utilize tow rear deriving wheel for motion can be improved using sliding mode control strategy based on space vector modulation when the battery developed power depend on the speed reference of the driver. The several speed variations do not affect the performances of the Nickel metal hydride battery and the control strategy gives good dynamic characteristics of the EV propulsion system. This paper proposes novel fitting formulas which give the relationship between the SOC and distance traveled and others formulas that give more efficiency to different propulsion systems paths.

References

- [1] M.Salman, M.Chang, J.Chen, “Predictive energy management strategies for hybrid vehicles”, *IEEE VPPC, Chicago, IL*, Sep. 7–9, pp. 21–25, 2005.
- [2] J.Larminie, J.Lowry, “Electric Vehicle Technology Explained”, *John Wiley and John Lowry*, England, 2003.
- [3] R.F.Nelson, “Power requirements for battery in HEVs”, *J. Power Sources*, vol. 91, pp. 2–26, 2000.
- [4] C.Xia, Y.Guo, “Implementation of a Bi-directional DC/DC Converter in the Electric Vehicle”, *Journal of Power Electronics*, vol. 40, no. 1, pp. 70–72, 2006.

- [5] Ramadass, P, et al., “Capacity fade of Sony 18650 cells cycled at elevated temperatures: Part II. Capacity fade analysis” *Journal of Power Sources*, 2002, Vol. 112, pp. 614 - 620. 0378-7753.
- [6] Q.Zhang, Y.Yin, “Analysis and Evaluation of Bidirectional DC/DC Converter”, *Journal of Power Technology*, vol. 1, no. 4, pp. 331–338, 2003
- [7] A. Gupta, A. M. Khambadkone “A space vector pwm scheme for multilevel inverters based on two-level space vector pwm,” *IEEE Transaction on Industrial Electronics*, Vol. 53, October 2006.
- [8] X.X.Yan, D.Patterson, “Novel power management for high performance and cost reduction in an electric vehicle”, *Renew. Energy*, 22, (1–3), pp. 177–183, 2001.
- [9] H.J.Chill, L.W. Lin, “A Bidirectional DC-DC Converter for Fuel Cell Electric Vehicle Driving System”, *IEEE Trans. Power Electron*, vol. 21, pp. 950–958, 2006.
- [10] T. G. Habetler, F. Profumo, M. Pastorelli, L. Tolbert “Direct torque control of induction machines using space vector modulation,” *IEEE Transaction on Industry Applications*, Vol. 28, no. 5, pp. 1045-1053, septembre/October 1992.